

High-resolution retinotopic maps estimated with magnetoencephalography



Konstantinos Nasiatou^{a,*}, Simon Clavagnier^b, Sylvain Baillet^a, Christopher C. Pack^{a,*}

^a Montreal Neurological Institute, 3801 University Street, Montreal, QC, Canada H3A 2B4

^b Montreal General Hospital, 1650 Av. Cedar, Montreal, QC, Canada H3G 1A4

A B S T R A C T

Magnetoencephalography (MEG) is used in clinical and fundamental studies of brain functions, primarily for the excellent temporal resolution it provides. The spatial resolution is often assumed to be poor, because of the ill-posed nature of MEG source modeling. However, the question of spatial resolution in MEG has seldom been studied in quantitative detail. Here we use the well-known retinotopic organization of the primary visual cortex (V1) as a benchmark for estimating the spatial resolution of MEG source imaging. Using a standard visual stimulation paradigm in human subjects, we find that individual MEG sources exhibit well-delineated visual receptive fields that collectively follow the known mapping of the retinal surface onto the cortex. Based on the size of these receptive fields and the variability of the signal, we are able to resolve MEG signals separated by approximately 7 mm in smooth regions of cortex and less than 1 mm for signals near curved gyri. The maximum resolution is thus comparable to that of the spacing of hypercolumns in human visual cortex. Overall, our results suggest that the spatial resolution of MEG can approach or in some cases exceed that of fMRI.

Introduction

Among the various methods for non-invasive imaging, magnetoencephalography (MEG) source imaging is known to provide outstanding temporal resolution, while it is typically assumed to have modest spatial resolution (Darvas et al., 2004; Hämäläinen et al., 1993). Consequently MEG imaging is most often used in experiments aimed at measuring temporal fluctuations in neural signals for which the assignment of a precise anatomical source is not critical. Although recent reports have raised the possibility of extracting rich spatial signals from MEG (Cichy et al., 2015), a quantitative estimate of the resolution that can be attained with this imaging modality is lacking.

Here we have examined the capacity of MEG to resolve the well-known retinotopic organization of the primary visual cortex (V1). This representation provides a useful benchmark, because it has been thoroughly and quantitatively characterized using a variety of methods, including electrophysiology (Das and Gilbert, 1995; Hubel and Wiesel, 1977), PET (Fox et al., 1987), optical imaging (White and Culver, 2010) and fMRI (Engel et al., 1997). These approaches have demonstrated a smooth change in the locus of cortical activation for corresponding changes in the position of the retinal stimulus (Dumoulin and Wandell, 2008; Engel et al., 1997; Sereno et al., 1995). Thus to the extent that an imaging modality has high spatial resolution, it should be able to differentiate responses to visual stimuli in different locations. The smallest shift in the locus of cortical

activation that can be detected serves as a measure of resolution.

Here we have obtained retinotopic maps from human subjects using MEG in combination with a standard visual stimulation paradigm. We show that surprisingly high spatial resolution maps can be obtained with appropriate choices of visual stimulation and source modeling. In particular, we are able to reliably detect distinct MEG responses emanating from sources separated by 7.0 mm along smooth cortical surfaces and less than 1 mm along the arched gyri.

Materials and methods

Participants

Data were recorded from two healthy, right-handed male subjects (one author, one naïve), both of whom had normal or corrected to normal vision. Both subjects gave written consent prior to participation in three sessions, involving structural MRI, functional MRI, and MEG recordings. All experimental protocols were approved by the Research Ethics Board of the Montreal Neurological Institute.

Structural MRI

For the MRI scans, each subject was positioned on his back with a 32 channel surface coil centered over the occipital pole. Three-dimensional T1-weighted anatomical MR image volumes covering the

* Corresponding authors.

E-mail addresses: konstantinos.nasiatou@mail.mcgill.ca (K. Nasiatou), christopher.pack@mcgill.ca (C.C. Pack).

entire brain were acquired on a Siemens TIM Trio scanner, prior to the functional scans (3D-MPRAGE, TR/TE= 2300/2.98 ms, TI=900 ms, 176 sagittally oriented slices, slice thickness=1 mm, 256×240 acquisition matrix).

fMRI data from Subject 1 (S1) and Subject 2 (S2) were originally collected for independent studies. A multi-slice T2*-weighted Gradient-echo echo-planar imaging (GE-EPI) sequence with slightly different parameters was used for S1 (TR/TE = 1940/30 ms, flip angle =76°, slice number=32 with no gap, slice thickness = 2 mm; 128×128 acquisition matrix, a 256×256 mm rectangular field of view (FOV) and GRAPPA (acceleration factor along Phase Encoding direction (PE) =3, reference lines=33) and S2 (TR/TE = 2000/30 ms, flip angle=76°, slice number=37 with no gap, slice thickness = 3 mm; 64×64 acquisition matrix, 192×192 mm rectangular FOV and GRAPPA. The slices were pseudo-coronally oriented perpendicular to the calcarine sulcus and covered the entire occipital lobe.

fMRI retinotopic experiment

The visual stimuli were generated with the Psychophysics Toolbox (Brainard, 1997; Pelli, 1997) and were back-projected on a screen outside of the bore at a viewing distance of 140 cm.

For S1, the stimulus consisted of a checkerboard pattern (100% contrast) visible through apertures of various orientations, as previously used for neuronal population receptive field (pRF) mapping (Clavagnier et al., 2015; Dumoulin and Wandell, 2008). The stimuli were viewed monocularly, with the dominant or the non-dominant eye being covered by a black patch alternatively on each run.

For S2, the stimuli consisted of 8 wedges (each subtending 45°) and 8 rings (each with a width of 1.38°) of a high-contrast moving dartboard pattern (Dumoulin and Wandell, 2008; Engel et al., 1997; Sereno et al., 1995). The 8 wedges and the 8 rings were successively presented for 2 s. The wedges were presented in a clockwise predictable order, and the rings of different eccentricities were sequentially presented in the expanding direction. The presentation followed a periodic pattern and completed a full cycle in 16 s with a total of 8 cycles per scanning run. The maximum stimulus radius was 11°, and all stimuli were viewed under binocular conditions.

In both cases, eye position was controlled by means of a fixation task (colored dot at the center of the visual field). The volunteer had to report, via a button press, the occurrence of a color change of the fixation target (from red to green or green to red). Each fMRI time series consisted of 106 (S1) or 60 (S2) measurements. Eight (S1) or four (S2) fMRI scans per eye were collected.

MEG data collection

Data were recorded using a 275-channel (axial gradiometers) whole-head MEG system (CTF MEG International Services Ltd.). Each subject's head was digitized (typically 200 points) with a 6 degree-of-freedom digitizer (Patriot - Polhemus) prior to MEG data collection. This was used to mark the scalp, eyebrows and nose, and to optimize co-registration with the anatomical MRI. Three head positioning coils were attached to fiducial anatomical locations (nasion, left/right pre-auricular points) to track head movement inside the MEG. Eye movements and blinks were recorded using 2 bipolar electro-oculographic (EOG) channels. EOG leads were placed above and below one eye (vertical channel) and the second channel was placed laterally to the two eyes (horizontal channel). Heart activity was recorded with one channel (ECG), with electrical reference at the opposite clavicle, for subsequent MEG artifact detection and removal. All data were sampled at 2400 Hz.

Visual stimuli were presented onto a screen placed in front of the subjects at a viewing distance of 45 cm, which permitted visual stimulation up to 25×20° of eccentricity. The display system consisted of a projector (Sanyo PLC-XP57L) located outside the magnetically

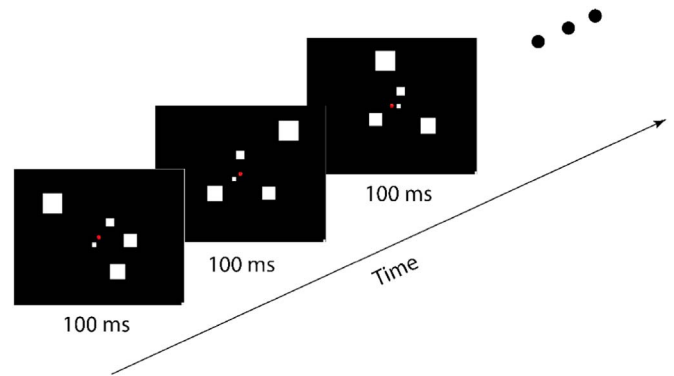


Fig. 1. Stimulus presented to the subjects to elicit visual responses. Squares with sizes scaled according to retinal eccentricity were presented in random positions that changed on each frame presented. Each frame was presented for 100 ms, and each run lasted 10 min.

shielded room and two reflecting mirrors that directed images to the screen. The refresh rate of the projector was 60 Hz with a resolution of 1280×1024 pixels.

Subjects were seated in a dimly illuminated room (0.13 cd/m²) and asked to fixate a red dot of 0.1° radius; the fixation point remained visible throughout the experiment. While the subject fixated, we presented stimuli comprised of multiple square probes positioned randomly within the central 20° of the visual field (Fig. 1). Probe stimuli on each frame were comprised of 5–15 squares (34.59 cd/m²) displayed at maximum contrast against the background (0.94 cd/m²). The width of each square was set to 30% of its distance from the fixation point, with the exception of those located at eccentricities less than 1°, which were forced to have a size of 0.3°. This scaling was chosen to approximate the size of receptive fields for neurons in V1 and V2 (Gattass et al., 1987; R Gattass, 1981). When a square overlapped with the fixation point, the latter was always presented over it, so the effective stimulation of that square was less than its area. Regions in which two squares overlapped were shown at the same luminance as individual squares. Each frame was presented for 100 ms with no time gap between frames. Since the screen's refresh rate was 60 Hz, each frame was presented for 6 monitor cycles.

Each subject participated in a single MEG session, comprised of 6 runs that lasted 10 min each. The sequence of stimulus frames was random within and across runs. Subjects were given a short break between runs.

To measure the actual timing of each stimulus presentation with respect to MEG data collection, we presented a small square at the bottom right corner of each frame. The luminance of the square changed on successive frames, and a photodiode was used to identify the exact time of occurrence of each stimulus frame, relative to the MEG signal.

Regions of interest

The primary visual cortex (V1) has the finest visual resolution among the visual areas in the occipital cortex, since its receptive fields are the smallest for each eccentricity (Burkhalter and Essen, 1986; Felleman and Essen, 1987; Gattass et al., 1987; R Gattass, 1981; Smith et al., 2001; Zeki, 1978). This makes V1 an ideal candidate for evaluating the resolution of MEG, since only a small part of the V1 cortex is expected to be activated with every localized stimulus on the visual field.

From the fMRI experiment, the cortical area of V1 was estimated and imported into the MEG data processing environment as a surface-based anatomical region of interest. Constraints on the visual stimulation available inside the MRI magnet led to limited coverage of the V1 maps for both hemispheres in both subjects. Given previous work

showing that higher eccentricities are represented more anteriorly along the calcarine sulcus (Dougherty et al., 2003; Dumoulin and Wandell, 2008; Engel et al., 1997; Sereno et al., 1995), we manually extrapolated our V1-fMRI maps anteriorly by including additional sources until the parieto-occipital fissure. The V1 maps, along with the extrapolated area, were selected as a region of interest for MEG source analysis.

MEG data analysis

MEG forward modeling was completed with the overlapping spheres approach (Huang et al., 1999). This method fits a sphere to the scalp surface under each sensor. A sphere can be used as a simplified model, since the magnetic fields are virtually undistorted by the skull (Barth et al., 1986; Okada et al., 1999).

Noise covariance across MEG sensors was estimated from a 2-min empty-room recording prior to the experiments. Weighted Minimum Norm Estimates (wMNE) (Lin et al., 2006) of cortically constrained, distributed sources were obtained using Brainstorm's default parameters (Depth weighting: 0.5, Regularize noise covariance: 0.1, Whitening: PCA / SNR: 3). Source orientations were constrained to be perpendicular to the cortical surface.

A high-resolution cortical tessellation (150,000 sources) was used from each subject's individual anatomy for creating the source model (Dale and Sereno, 1993). This approach caused sources to have, in most cases, less than a millimeter distance from their closest neighbors, providing the possibility of detecting variations in the MEG signal on small spatial scales.

The inverse modeling transforms the signals from 275 sensor-signals, to 150,000 sources-signals. This leads to a vast amount of data. In order to decrease the volume of data, the signals were down-sampled to 600 Hz, and only the time-series from the sources located inside the V1 regions of interest (as described above) were considered for further analysis (4890 sources for S1 and 5311 sources for S2). The signal of each source was epoched into 1-min bins, and the baseline (time average) of each epoch was subtracted. In order to reduce the contribution of heartbeat artifacts, signal space projection (Tesche et al., 1995; Uusitalo and Ilmoniemi, 1997) was applied to the MEG signals prior to source modeling.

Estimation of visual receptive fields

The epoched time-series from the sources located in the region of interest were band-pass filtered (4th order Butterworth filter) in the 1–12 Hz range (Fig. 2). This range was chosen from analysis of pilot data from our lab showing strong, evoked visual responses in this frequency range from sources located in V1 (Appendix 1). Within this range, evoked visual responses were almost always biphasic (Appendix 2, (Aine and Stephen, 2003; Kaoru Seki, 1996; Nakamura et al., 2000; Stephen et al., 2002), with the leading phase varying across sources.

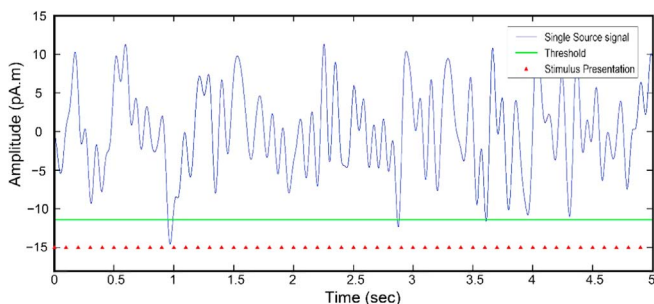


Fig. 2. Example of a 5 s segment of signal from an occipital source, filtered between 1 and 12 Hz. The line in green indicates the threshold of 3 standard deviations below the mean of the filtered signal that was used for detection of selective visual responses. The red triangles indicate the time points at which the stimulus was updated.

In order to identify the responses associated with individual stimulus frames, we set a threshold of three standard deviations below the mean response of each epoch (Fig. 2, green line). The negative polarity of the response was chosen arbitrarily; using the positive phase of the response yielded results that were nearly identical to those reported here. On average ~3% of the total frames presented during the experiment led to threshold crossings in the filtered single-trial MEG responses for both subjects.

For each significant response that crossed the threshold on a given source, we took the average value of each pixel on the screen during the preceding two frames (200 ms). This procedure is equivalent to the reverse correlation analysis commonly used to study receptive fields in individual neurons (de Boer and Kuyper, 1968; DeAngelis et al., 1995; Livingstone et al., 2001; Marmarelis and Marmarelis, 1978; Mineault et al., 2013; Pack et al., 2006). The resulting spatial maps were then summed across all significant responses for the same source, to yield that source's receptive field map. This map was then normalized by the frequency with which each pixel was activated during the experiment. Because the most peripheral pixels were activated very infrequently, this normalization introduced discontinuities near the edges of the display screen. We therefore cropped each response-triggered average at ~16 degrees of eccentricity. The analysis was performed for every source individually. In order to avoid artifactual responses, we rejected epochs in which blinks were detected in the EOG.

Statistical significance of receptive fields

An anisotropic 2D Gaussian function was fit to each source's responses, to estimate the center of the receptive field and its spread along the two visual field axes:

$$f(x, y) = A \exp(-a(x - x_0)^2 - 2b(x - x_0)(y - y_0) + c(y - y_0)^2), \quad (1)$$

$$\text{where } a = \frac{\cos^2 \theta}{2\sigma_x^2} + \frac{\sin^2 \theta}{2\sigma_y^2}, \quad b = -\frac{\sin 2\theta}{4\sigma_x^2} + \frac{\sin 2\theta}{4\sigma_y^2}, \quad c = \frac{\sin^2 \theta}{2\sigma_x^2} + \frac{\cos^2 \theta}{2\sigma_y^2}$$

Here A is the amplitude, x_0, y_0 represent the center, and σ_x, σ_y the standard spread of the Gaussian kernel. The angle θ denotes the clockwise rotation applied to the elliptical function to fit the data.

In order to verify that receptive fields were not due to random signal fluctuations, we compared the amplitude (A) of the Gaussian fit to a threshold that was defined through a permutation test (Pack et al., 2006). We used the same number of frames that were averaged to create the receptive field, but shuffled the order of the stimuli. The resulting receptive field was fit again to a 2D Gaussian function, and the amplitude of this Gaussian was compared to the one that was computed from the experimental data. This procedure was repeated 1000 times. Significant receptive fields were considered as those that had higher amplitude than 95% of those calculated through the permutation.

The distance between the fixation point and the center of the Gaussian fit provided the eccentricity of each source's receptive field. For the sources that demonstrated significant receptive fields, the value of their eccentricity was assigned to each source's cortical location. For display purposes, the eccentricities were grouped into 3 different ranges: 0–2, 2–5, 5–11 and were color-coded for projection onto the cortical surface.

Comparison of MEG with fMRI results

For comparing the receptive fields that were obtained from the two modalities, for each hemisphere of the two subjects, we selected a line along the upper lip of the calcarine sulcus, thus sampling a wide range of eccentricities (Engel et al., 1997). For the MEG data points, only the sources that belonged on this line and demonstrated significant receptive fields were taken into account for the comparison. In order to generate a representation of the change of the visual field representation on the cortical surface, a source of 5.8° of eccentricity was

selected as the reference. This eccentricity was selected as a reference because all lines from the 4 hemispheres demonstrated a source at 5.8° with significant receptive fields. The eccentricity of each source on those lines was plotted relative to the geodesic distance between the references and every other source. The geodesic distance was computed with the fast-marching algorithm (Sethian, 1996). The fast marching algorithm is very similar to the Dijkstra algorithm (Dijkstra, 1959) that is used in graph theory to find the shortest paths on graphs.

The fMRI points were computed on 2-dimensional, flattened representations of the cortical manifold centered on the foveal confluence and subtending 100 mm of diameter. Linear ROIs were manually drawn within V1 to match as closely as possible those already determined on the MEG-based data, one per each hemisphere. The linear ROI was made of equidistant (on the flat maps) cortical bins that were assigned the average of the eccentricity values of the voxels they contained. The numbers of bins depended on the length of the line. Linear cortical magnification factor was estimated after calculating the geodesic cumulative distance between the bins (with the origin arbitrary set at 5.8°) and plotting them against their main eccentricity.

Spatial resolution

For the calculation of spatial resolution, we used data comprised of the threshold crossing of each individual source that demonstrated a significant receptive field. The total number of frames in the experiment was 36,000, and a binary vector (1×36,000) was created for each source indicating on which frame the source response passed the threshold. Consequently, for any two sources with significant receptive fields, we formed a 2×36,000 matrix. For two sources with identical visual responses, the two rows of this matrix would be identical, which would in turn imply that we were unable to resolve signals at the corresponding inter-source distance.

To quantify resolution, we therefore performed a singular value decomposition (SVD) on that binary matrix and obtained 2 singular values (s_1 and s_2) that expressed the separability between the two vectors. When the two vectors are identical, only the first singular value is representative of the matrix, and the second value is zero. This would correspond to an inability to resolve differences between the two sources. On the other extreme, when the two vectors have their values completely non-overlapping, the two singular values are equal. The separability index (SI), given by $SI = \frac{s_1^2}{s_1^2 + s_2^2}$, is therefore indicative of the degree of overlap between the two binary vectors and representative of the correlation among sources. The SI thus ranges from 0.5, when responses are completely independent, to 1.0, when responses are identical. The advantage of using the singular values ratio, compared to the dot product between the two vectors, is that the former is affected by instances when only one of the two sources crosses the threshold, which was often the case in our data.

In order to establish the SI values that would be expected based on pure noise, we described the probability of having concurrent threshold crossings for every pair of sources. This probability is based on the number of frames to which each source showed selectivity and the total number of frames presented. We estimated the cumulative probability of concurrent threshold crossings and included in the plot only the data points that were above the 95% distribution, which was set as the noise level.

The probability of having α concurrent threshold crossings based on chance is defined by a hypergeometric distribution:

$$\text{noise distribution} = \frac{\binom{v_1}{\alpha} \binom{TF - v_1}{v_2 - \alpha}}{\binom{TF}{v_2}} \quad (2)$$

where v_1 and v_2 are the number of frames on which the first and the second source surpassed the frame selectivity threshold respectively,

TF is the total number of frames (36,000), and α is the number of concurrent threshold crossings ($\alpha \in [0, \min(v_1, v_2)]$). From this distribution we calculated the cumulative distribution for setting the noise threshold at 95%.

For each combination of sources with significant receptive fields in the same hemisphere, we plotted the SI relative to their geodesic distance and their relative orientation, creating a 3 dimensional plot. The data points were binned into 1 mm by 2° bins, extending from 0–80 mm and 0–180°, for the observed geodesic distance and orientation values respectively. Since not all bins had the same number of data points, we fit the data-points to a 2-dimensional exponential function, weighted by an inverse multivariate kernel density estimator (Hwang et al., 1994):

$$f(d, \theta) = \alpha_0 + ae^{(bD+c\theta)} \quad (3)$$

Here D is the geodesic distance between sources, and Θ the relative orientation between the sources. α_0 is a constant that captures the baseline (0.5) and common noise among sources, α is the amplitude and b and c are constants that capture the decay of the exponential function for the distance and orientation axes.

The threshold for defining the resolution is based on the decay constant of the exponential function that was used to fit the data points. Since the exponential is 2-dimensional, the threshold is a line that relates geodesic distance and relative orientation between sources. The decay constant shows the space-angle combinations that are needed for the correlation to drop to 1/e (36.8%) of its maximum value. The line that defines this threshold can be interpreted as the point where the responses of the two sources are 63.2% separable. The threshold is given by the equation:

$$-1 = bD+c\theta \quad (4)$$

The placement of the sources on the cortical surface, and therefore the geodesic distance and the relative orientation between them, is affected by the curvature of the surface. For examining the possible placements for given curvatures, we assumed for simplicity that the local cortical surface could be approximated by an osculating sphere with radius: $R = 1/\text{curvature}$ (DoCarmo, 1976). The combinations of the orientation and perimetric distance of sources that can be placed on a sphere form a line that follows:

$$d = \frac{2\pi\theta}{360 * \text{Curv}} \quad (5)$$

where d is the distance between the two dipoles along the curve of the osculating sphere, θ is the relative angle between the dipole sources, and Curv is the curvature of the sphere (1/Radius of the sphere). By solving the linear system of Eqs. (4) and (5), we can derive the maximum resolution that MEG can achieve for surfaces with given curvatures.

Software

MEG data analysis was performed with Brainstorm (Tadel et al., 2011). Cortical reconstruction and volumetric segmentation were performed with the Freesurfer image analysis suite (<http://surfer.nmr.mgh.harvard.edu/>) (Dale et al., 1999; Fischl et al., 1999, 2001).

Results

We studied the spatial properties of MEG signals emanating from the visual cortex in two human subjects. We elicited visual responses by presenting images comprised of a small number of squares flashed simultaneously on a computer monitor. In this section we analyze the relationship between the positions of individual stimulus squares and MEG source responses, as well as the distribution of these receptive fields across the cortical surface; we use these data to derive an estimate of the overall resolution of MEG source imaging.

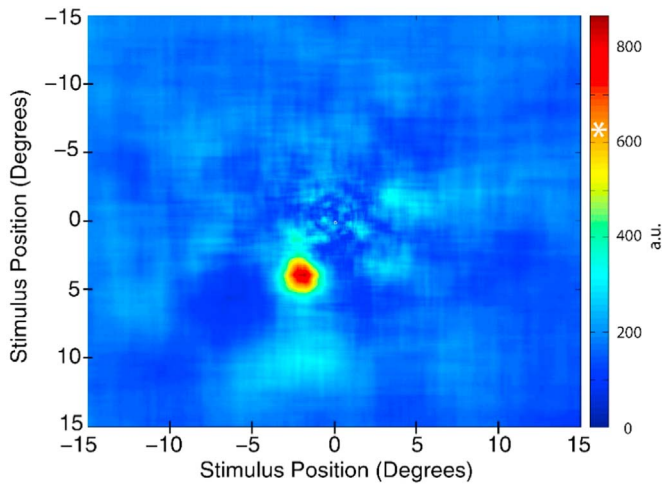


Fig. 3. Example of a receptive field calculated from a single cortical source. This source belonged to the right hemisphere and was located above the calcarine sulcus in the primary visual cortex. The white star on the color bar defines the limit, above which the receptive field was deemed significant.

Visual receptive fields estimated from individual occipital sources

Based on the stimulation procedure illustrated in Fig. 1, we were able to recover discrete visual receptive fields for individual MEG sources. These receptive fields were obtained by reverse correlating (de

Boer and Kuypers, 1968; Ringach and Shapley, 2004) the source responses and the stimuli (see Methods). The results described below were based on receptive field estimates obtained with 60 min of data collection, although comparable results can be obtained with far less data (Appendix 3).

Fig. 3 illustrates the receptive field that was calculated for a single source located in the right hemisphere in area V1 of subject 1. The origin of this plot corresponds to the position of the fixation point. For this source there was a well-localized receptive field located at a retinal eccentricity of 4.3°; as expected from a source located in the right hemisphere, its receptive field was in the left visual field. The radius of the receptive field for this source was 1.4°, which is about 10 times bigger than what previous studies have demonstrated for individual V1 neurons (Gattass et al., 1987; R Gattass, 1981; Van Essen et al., 1984) and about 2 times bigger than V1 population receptive fields obtained with fMRI (Dumoulin and Wandell, 2008). This suggests that the spatial resolution of MEG, while somewhat coarse, can be comparable to that of other imaging modalities. However, as shown below, MEG spatial resolution varies substantially with source orientation.

Retinotopic maps estimated with MEG

The visual cortex is organized into visual maps, so that nearby neurons encode nearby regions of visual space (Dumoulin and Wandell, 2008; Engel et al., 1997; Holmes, 1945; Horton and Hoyt, 1991; Sereno et al., 1995). That is, for a given change in cortical location, one finds a predictable change in the retinal position encoded

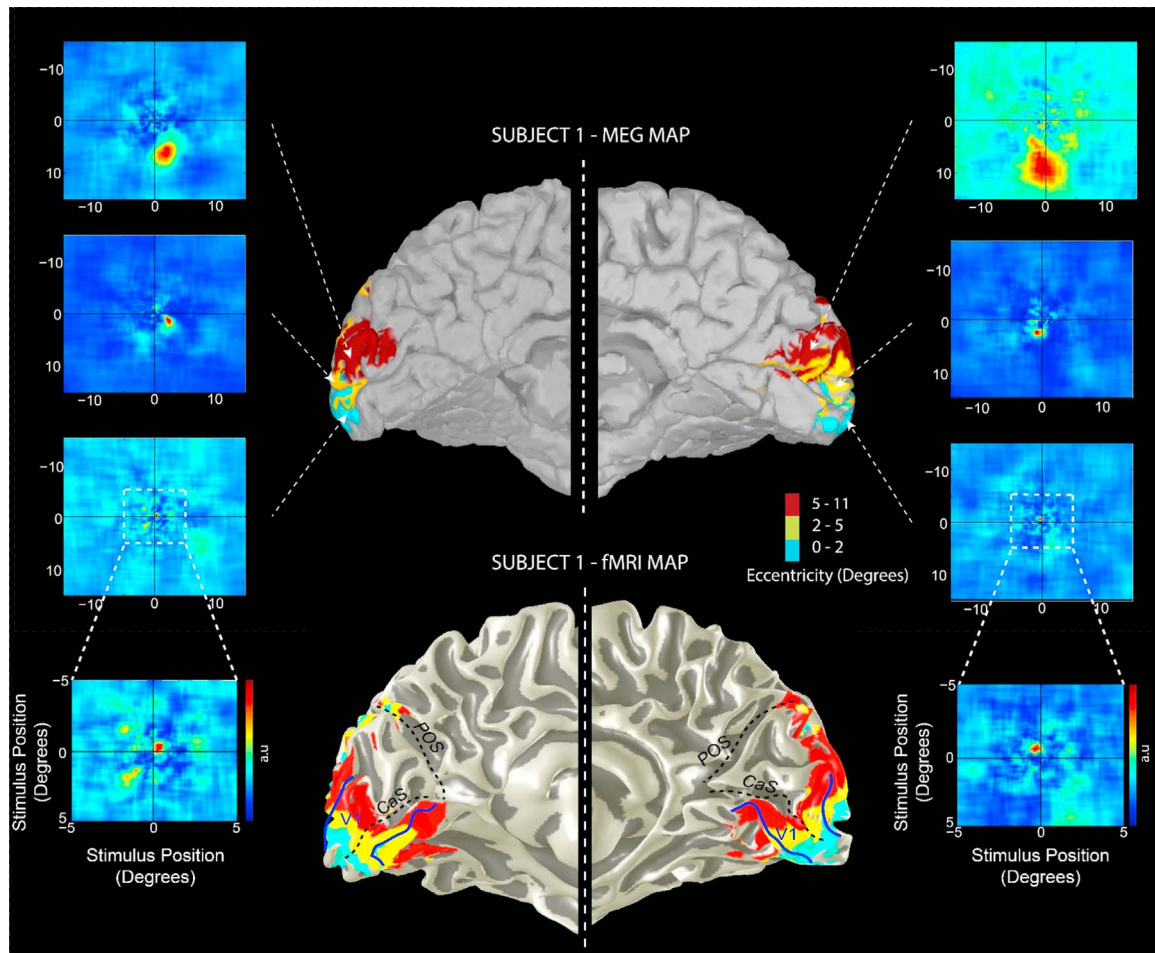


Fig. 4. Example receptive fields taken from different positions in the V1 retinotopic map (left and right panels). The foveal example receptive fields are expanded for better visualization. Full retinotopic maps are shown for MEG (top) and fMRI (bottom) for subject 1. Only sources that formed a cluster of 3 or more sources and all of them demonstrated receptive fields are projected.

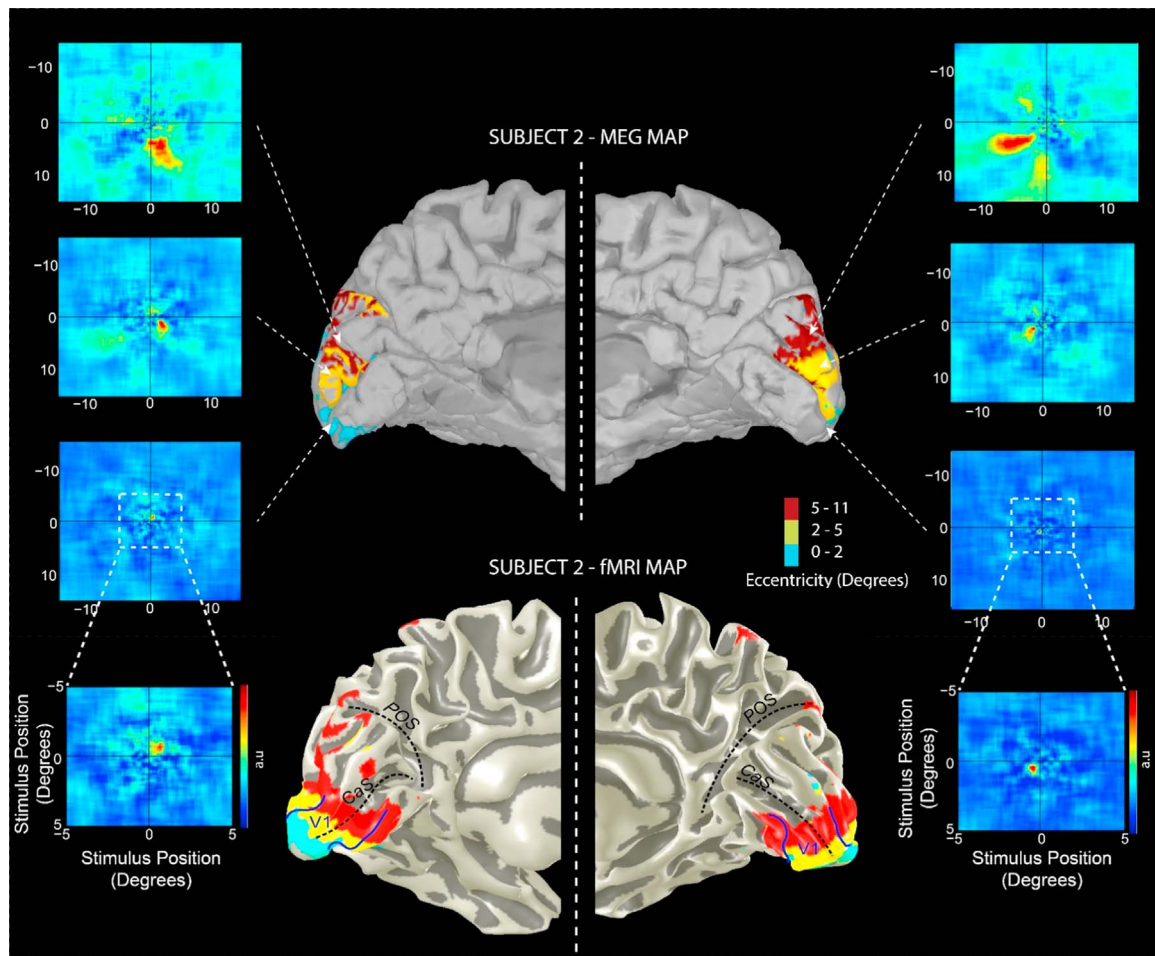


Fig. 5. Same as Fig. 4, but for subject 2.

by that location. In order to estimate this relationship in our MEG data, we calculated the physical location and the retinal eccentricity associated with each MEG source.

The physical location of each source was estimated from structural MRI images for each subject, from which we created cortical surface reconstructions (Dale and Sereno, 1993). The calculation of the receptive fields was performed only on the sources that were located inside the regions of interest. Within these regions we computed 4,890 receptive fields for subject 1 and 5,311 for subject 2. For every computed receptive field, a 2-D Gaussian function was fit to the data and significance testing was conducted (see Methods).

For both hemispheres in both subjects, there was a fairly smooth gradation of the eccentricities of the significant receptive fields along the upper lip of the calcarine sulcus in area V1. The sources that had foveal responses were clustered at the most posterior part of the cortex, and those with higher eccentricity were located more anteriorly, as expected from known retinotopic organization (Wandell et al., 2007).

Figs. 4 and 5 depict the individual MEG retinotopic maps based on eccentricity. The eccentricity values were binned into 3 categories, and an example receptive field from one source from each eccentricity category is displayed next to the maps for each hemisphere for both subjects. The figures also show the occipital eccentricity maps that were calculated from the subjects' fMRI data. Separate maps that show the polar angle are depicted in Appendix 4 and 5.

The individual receptive fields for the example sources indicate localized spatial selectivity in the positions and sizes of the receptive fields. The foveal sources exhibited clear receptive fields at eccentricities as small as 0.34° ; this was the smallest eccentricity for which receptive fields could be reliably estimated, given the 0.15° extent of

the fixation point. The maps also indicate a precise mapping of visual inputs to the contralateral hemisphere, with very little spread of receptive fields across the vertical meridian (Jeffreys and Axford, 1972). As expected, the receptive fields were larger for more peripheral sources.

Estimate of cortical magnification factor with MEG

In order to draw a more quantitative comparison between the maps obtained with MEG and those obtained with other methods, we computed the cortical magnification factor for V1 in each individual hemisphere, using the full 60 min of data for each experiment. Cortical magnification corresponds to the amount of cortical space devoted to a given portion of the retinal input: Notably, previous work has shown that the central visual field is represented by a larger area compared to periphery (Daniel and Whitteridge, 1961).

To quantify cortical magnification across the retinotopic maps recovered previously, we selected sources located on a line running along the upper lip of the calcarine sulcus for all 4 hemispheres of the two subjects (Engel et al., 1997). The line was chosen to sample the range of eccentricities shown in Figs. 4 and 5.

Fig. 6A plots the location of each receptive field as a function of the position of the corresponding source. Here position is referenced to a single source with a receptive field at an eccentricity of 5.8° (Engel et al., 1997 used 10°). Relative to more foveal sites, stimulation at 5.8° activates a small portion of the visual cortex, which facilitates more accurate alignment across subjects and across hemispheres.

Each point in Fig. 6A corresponds to a source with a significant receptive field. Negative values on the x -axis correspond to sources

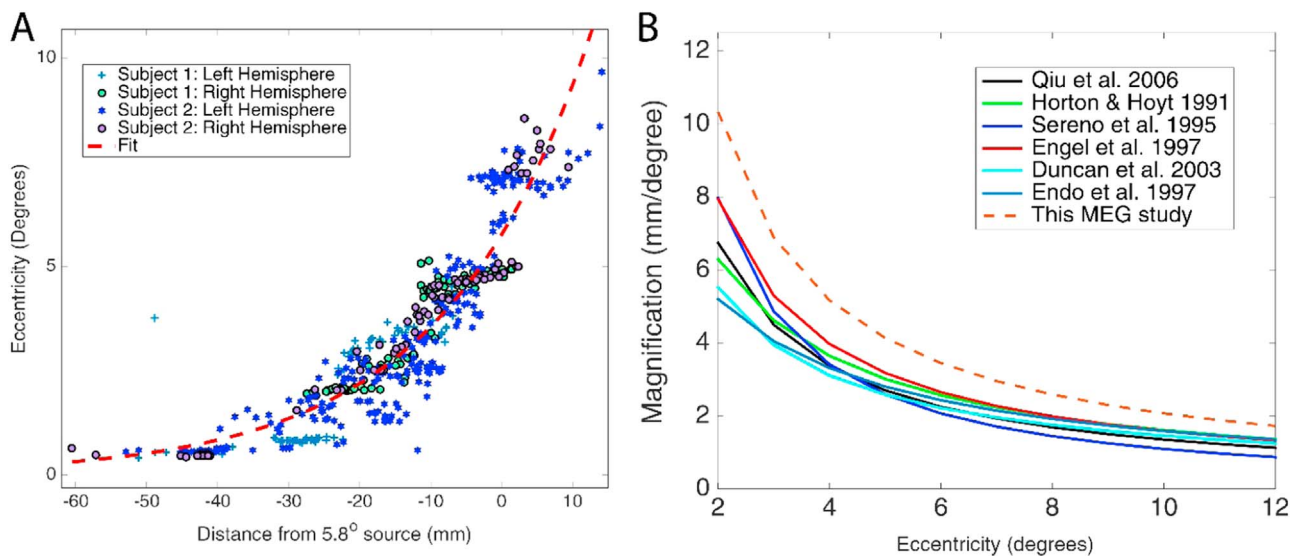


Fig. 6. (A) Visual field eccentricity as a function of distance from the 5.8° source in V1 for all 4 four hemispheres of the two subjects. The sources were selected from a line that runs along the upper lip of the calcarine sulcus. The different shapes and colors of the data points indicate the hemisphere to which they belong. The dashed red line represents the fit to the data. (B) Comparison of the cortical magnification factor among the present and previous studies.

located posterior to the 5.8° eccentricity point, and positive values indicate more anterior sources. The x-axis of the plot represents geodesic distances between the sources on the cortical surface.

The results indicate a consistent trend across hemispheres and across subjects. Near the posterior end of the occipital cortex (leftmost points in Fig. 6A), changes in cortical location yield very small changes in the retinal location of the corresponding receptive fields; in other words, the central region of the retina is represented by a relatively large amount of cortical space, as reported with other methods (Duncan and Boynton, 2003; Endo et al., 1997; Engel et al., 1997; Horton and Hoyt, 1991; Qiu et al., 2006; Sereno et al., 1995). In contrast, sources located more anteriorly (rightmost points in Fig. 6A) are associated with less cortical tissue; small changes in retinal position yield large changes in cortical position.

These trends can be captured parametrically by an exponential function that relates increases in retinal eccentricity distances on the cortical surface. To explore this relationship, we fit a function of the form: $\theta = e^{c(d+d_0)}$ (6) (Engel et al., 1997), where θ is the eccentricity of the receptive field for the source, d the cortical distance, and c and d_0 are parameters that scale and shift the exponential relationship. The mean values of the parameters obtained were: $\theta = e^{0.04*(d+40.01)}$. From these values we obtained the linear magnification factor, which has units of millimeters of cortex per degree of visual angle: $M(\theta) = (\frac{1}{c})\theta^{-1}$ (Qiu et al., 2006). From our data, the corresponding relationship is $M(\theta) = 21.14\theta^{-1} \text{mm/degree}$. These values are plotted in Fig. 6B (Brown dashed line), along with analogous functions from previous studies.

The shape of M found from our data is similar, although with a clear upward shift with respect to that obtained with fMRI and PET (Duncan and Boynton, 2003; Engel et al., 1997; Horton and Hoyt, 1991; Qiu et al., 2006; Sereno et al., 1995).

Comparison with fMRI

To compare the results that we obtained from the MEG analysis to those obtained in the same subjects with fMRI, we selected the same lines along the calcarine sulcus that were selected for creating Fig. 6A for each of the 4 hemispheres. These are overlaid with the data points from the fMRI results in Fig. 7. Only the data points for MEG sources with significant receptive fields were included on the plot. Overall the results indicate a close correspondence between the retinotopic organization obtained with MEG (red dots) and with fMRI (blue stars) in all hemispheres.

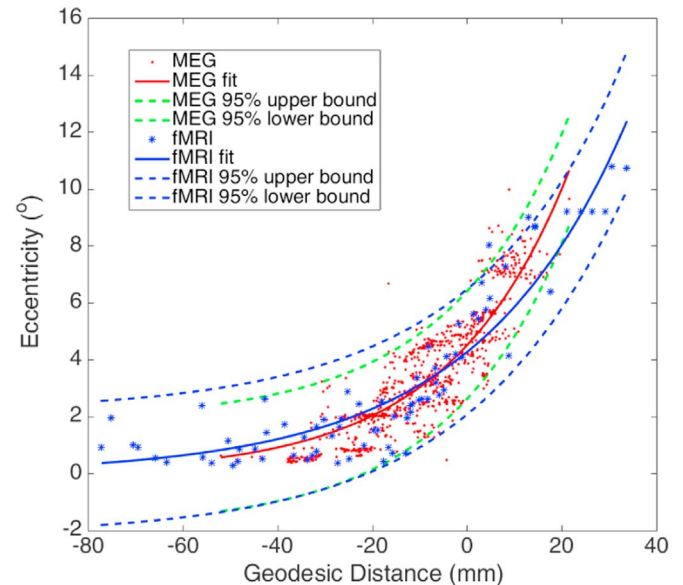


Fig. 7. Comparison between MEG (red dots) and fMRI (blue stars) data for the 4 hemispheres. Data points were selected along linear regions of interest that run along the upper lip of the calcarine sulcus. The green and blue dashed lines correspond to the 95% significance bounds for MEG and fMRI exponential fits respectively.

Spatial resolution of MEG

We used the pattern of visual responses and source locations described above to estimate the spatial resolution of MEG. Conceptually one can characterize spatial resolution as the minimum physical separation of sources that reliably yields different visual responses. Given the convoluted nature of the cortex, we expect this measure of resolution to differ depending on the position of each source relative to individual sulci and gyri. We therefore estimated spatial resolution separately for sources of different orientations. For this analysis, we considered all sources for which statistically significant receptive fields could be recovered (see Methods).

We developed a metric of correlation (SI; see Methods) that takes into account the responses of each source to each frame of the visual stimulus presentation. This metric takes values near 1.0 for sources that have identical responses across all stimuli to 0.5 for sources that

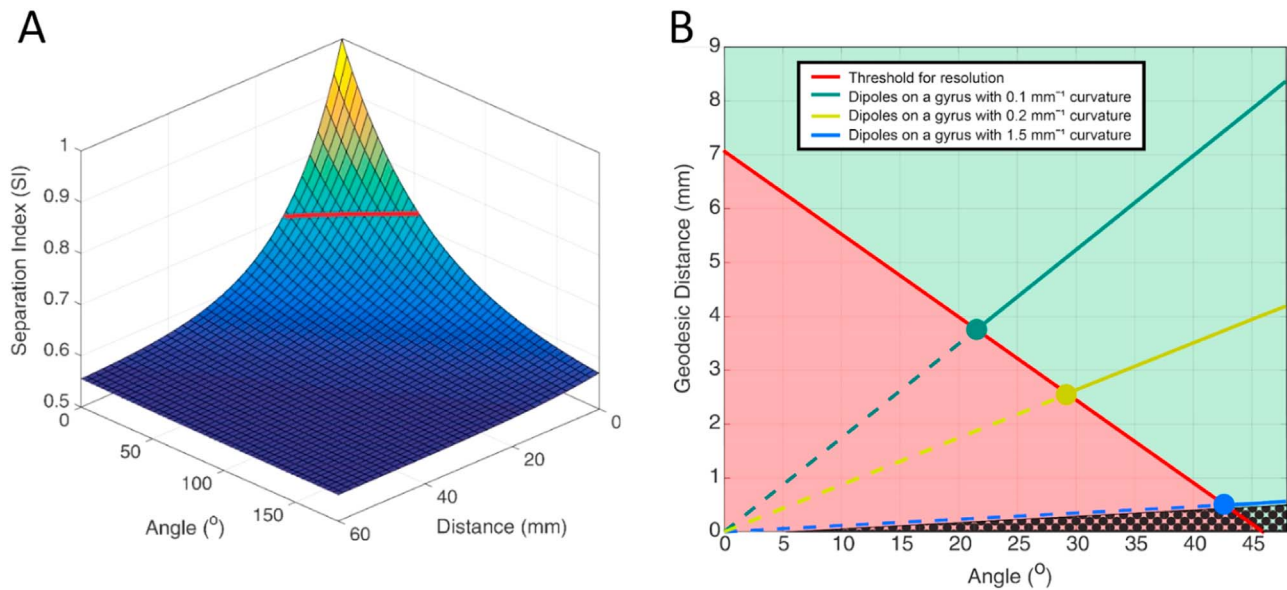


Fig. 8. (A) 2-dimensional exponential fit of the separation index (SI) as a function of spatial separation and relative orientation of pairs of sources. The correlation decreases along both dimensions, and the decay constant (red line) is taken as a measure of resolution. (B) Different combinations of geodesic distance and relative orientation between sources influence the separability among responses. The red line represents the red line in Fig. 8A. The area marked in red represents the combinations that are beyond the resolution of MEG, and the green area the combinations that MEG can resolve. The dark patterned area represents observations that are within the noise level of the MRI tessellations. The other colored lines represent resolution for dipoles placed near gyri with different curvatures. The blue line shows the combinations on a gyrus with the maximum curvature typically found in human brains; this therefore represents the limit of MEG resolution.

respond completely independently. We estimated this correlation for all pairs of sources, combining data for sources separated by similar geodesic distances and relative orientations.

The pairwise value of this correlation is plotted in Fig. 8A, as a function of geodesic proximity and relative orientation between sources. As expected, the responses of nearby sources with similar orientation are highly correlated, and this correlation decreases with increasing differences in spatial position or orientation. In the limit, the pairs of sources are nearly completely independent, as sources that are physically far apart respond to stimuli that are widely separated in retinal space.

We estimated the spatial resolution of MEG as the decay constant of an exponential fit to the correlation functions obtained in our data (see Methods and Fig. 8A) (Adjusted R^2 : 0.68). The results show that for sources with the same orientation (i.e. cortical regions along a relatively flat region of a sulcus), responses can be reliably differentiated when they are separated by approximately 7.0 mm. For regions of greater curvature (i.e. near a gyrus), resolution can be considerably greater. The red line in Fig. 8B indicates that the decay constant is reached at smaller physical separations for dipoles of increasing relative orientations. Assuming a maximum curvature of 1.5 mm^{-1} that can be measured before reaching the noise level of the MRI measurement on a $1 \times 1 \text{ mm}$ isotropic space (Pienaar et al., 2008), this calculation yielded a maximum MEG resolution of 0.49 mm (blue line). For regions with more modest curvature (green and yellow lines in Fig. 8B), resolution was on the order of 2–4 mm.

Of course, any estimate of resolution will depend on various experimental and analytical choices. Although we did not explore these factors exhaustively, we performed one additional analysis to explore the influence of response threshold (see Methods). A lower threshold (2 standard deviations below the mean) admitted far more responses into our receptive field measurements, but lowered the resolution significantly, yielding values of 41.3 mm and 105.0° for the space and orientation constants. By comparison, a threshold of 4 standard deviations yielded a space constant of 3.6 mm, and an orientation constant of 52.5° . Although this resolution was slightly better than what we obtained with the 3 standard deviations threshold, it led us to reject 97% of the data that was used in the 3 std threshold condition.

Thus the higher threshold might be warranted for experiments with rich data records, if extra resolution is necessary.

Discussion

Brief summary of results

In this study we have demonstrated the capacity of individual MEG sources to show selectivity for specific areas of the visual field. We showed that localized visual receptive fields for individual sources (Fig. 3) can be obtained from modest amounts of data (Appendix 3), and that the ensembles of these receptive fields form orderly maps within the occipital lobe (Figs. 4 and 5). These maps are well matched to those obtained with fMRI (Fig. 7). Analysis of correlated responses between pairs of sources suggest a reliable resolution on the order of a few millimeters, with the precise number depending on local brain curvature (Fig. 8).

Comparison to previous work

The resolution of any imaging modality depends on a combination of the instrument and the analysis methods. For MEG, an important aspect of data analysis is the set of assumptions needed to reach a unique solution (Baillet et al., 2001; Hämäläinen and Ilmoniemi, 1994; Hämäläinen et al., 1993; Pascual-Marqui et al., 1994; Sarvas, 1987) to the electromagnetic inverse problem (Helmholtz, 1853). These require a method for modeling the source of MEG signals.

Traditionally, two approaches for modeling brain activity have been used: dipole methods, and imaging methods. Dipole methods make use of a small number of dipoles to explain the cortical activity in the simplest possible way. Although they achieve seemingly point-like localization, these models are restrictive, and an imaging method is preferred when the number of active regions cannot be predicted or large areas are activated (Benbadis et al., 2010; Darvas et al., 2004). An imaging method with distributed sources along the cortex is generally expected to provide coarse resolution due to the largely underdetermined character of the inverse problem: the model transforms the signals from a few hundred sensors to tens of thousands of sources on

the cortex. Nevertheless, imaging methods provide a more realistic representation of the cortex and are more suitable to account for spatially extended cortical activations. When the activated areas are in close cortical proximity, the localization of the sources becomes problematic, resulting in crosstalk between nearby sources (Liu et al., 2002). The minimum distance required to overcome this crosstalk provides one estimate of the spatial resolution of MEG.

Previous studies focused on the localization accuracy of MEG, which is the cortical distance between a “ground truth” cortical location, and the center of mass or peak of the MEG activation. The cortical points that are selected as the true origin of the activity are usually cortex locations that show increased activation in equivalent fMRI experiments (Moradi et al., 2003; Poghosyan and Ioannides, 2007; Sharon et al., 2007), locations that have been chosen in simulations (Liu et al., 2002), dipole localization in phantom studies (Leahy et al., 1998; Sutherling et al., 2001) or even dipoles that were placed inside a cadaver head (Barth et al., 1986).

Although previous MEG studies have examined the visual cortex, none to our knowledge has attempted to recover detailed retinotopic maps. Two previous studies demonstrated differentiation in response timing across entire visual areas (Cottureau et al., 2011; Hagler et al., 2009), while another study (Sharon et al., 2007) used several inverse methods to compare localization of fMRI and MEG+EEG from only 4 visual field stimuli positions. Cicmil et al. (2014) used 3 different inverse problems (MNE, Beamformers and Multiple Sparse Priors) with quadrant checkerboards and rings of 3 different eccentricities, and concluded that significant improvement could be achieved by using MNE on eccentricity stimuli confined to one visual field quadrant. Another study (Brookes et al., 2010) used a retinotopic experiment of 5 wedges and investigated the effect of data averaging from a retinotopic experiment on the spatial specificity of MEG. Moradi et al. (2003) compared MEG early activation with fMRI in V1 and achieved localization errors on the order of just 3–5 mm. Perry et al. (2011) used a rotating checkerboard stimulus and examined the elicited power at gamma frequencies, which did not yield a trajectory consistent with V1 anatomy. Poghosyan and Ioannides (2007) displayed circular checkerboards in 8 positions of the visual field and achieved localization in each visual cortex area to within 2mm of a simulated activation center.

Several previous MEG tonotopy studies have used sharp responses (namely the M100) for detecting selectivity (Cansino et al., 1994; Langner et al., 1997; Pantev et al., 1988, 1994, 1995). It would be interesting to use the method described in this paper to retrieve the tonotopic organization of the auditory cortex.

Limitations of current results

The method for computing the receptive fields that was described in this paper led to the creation of retinotopic maps that follow the known retinotopic organization of the primary visual cortex, on the upper lip of the calcarine sulcus. However, this technique was unable to capture many sources with significant receptive fields in the upper visual field (see Appendix 4 and 5); these are located below the calcarine sulcus. One reason for this might be the fact that every stimulus frame was comprised of several squares that were projected onto both the upper and lower visual field. Since it has been reported (Fylan et al., 1997; Perry et al., 2011; Poghosyan and Ioannides, 2007; Portin and Hari, 1999) that the signals from upper visual field stimulation are weaker than those from the lower visual field, it might be that their event related responses were not strong enough to cross the amplitude threshold.

A second limitation is that our retinotopic maps detected few significant receptive fields inside the sulci. This becomes evident when we project the maps onto an inflated cortex (Appendix 6). This leads to the appearance of discontinuities on the gradient of the eccentricity map for both subjects. These results are consistent with previous work

showing reduced signal strength for sources located inside sulci (Goldenholz et al., 2009). Consistent with this idea, we found in pilot studies that the ratios of the peak z-scored signal fluctuations relative to pre-stimulus baseline (Appendices 1–3) were higher in the upper lip of the calcarine sulcus (1.18) than in the lower lip (1.05) or the inside the sulcus (1.00). Since the method for estimating receptive fields is solely based on amplitude thresholding, the lack of significant results in the upper visual field is likely due to relatively poorer signal strength in the corresponding cortical space.

Another limitation was that significant receptive fields were mostly recovered in the primary visual cortex, and our attempts to recover retinotopic maps in extrastriate areas were less successful. We also did not detect the borders between areas V1, V2, and V3 that typically appear as inversions of the angle of visual field selectivity (Dougherty et al., 2003; Sereno et al., 1995; Wandell et al., 2007). One possible explanation is that we filtered our data (Fig. 2) at frequencies specifically chosen to optimize V1 responses. This filtering might have been optimal for capturing large signal fluctuations on V1 sources but not necessarily for others. Similarly, we optimized our stimuli based on estimates of receptive field sizes in early visual areas (Freeman and Simoncelli, 2011). Presumably, for any visual area, using larger stimuli would yield poorer resolution, while smaller stimuli would yield weaker responses, although we have not explored this trade-off experimentally.

MEG usage is beneficial in areas where the fMRI signal gets distorted due to large blood vessels

The fMRI signal can be affected by the presence of large blood vessels in certain areas due to the inflow effect (Gao and Liu, 2012). Consequently retinotopic maps in our fMRI experiment had small patches in which the signal could not be resolved reliably. Those areas were located on the most posterior part of the cortex for both subjects. Nearby voxels showed selectivity for stimuli presented at eccentricities less than one degree, suggesting that the missing patches also represented the central part of the visual field. Because MEG measures neuronal activity directly, it is not perturbed by large vessels, and thus we were able to resolve cortical activity in these regions (Figs. 4 and 5). This suggests that MEG can provide information that is complementary to that obtained with fMRI.

Resolution

Our results show that the resolution is affected by both the distance and relative orientation among sources (Fig. 8). Thus we expect spatial resolution to be quite different for sources located around gyri, within the sulci (see above), and in flatter areas. Given optimal brain curvature and sensory stimulation, MEG can detect differential selectivity between sources that are physically very close. However, for flatter regions of cortex, the resolution is likely to be substantially worse than that of fMRI. Therefore smoothing of the retinotopic maps obtained with MEG is helpful for comparing between the two modalities.

Findings of differential selectivity for sources in very close proximity have been reported recently (Cichy et al., 2015), in a study in which the authors investigated the ability of MEG to discriminate between distributed simulated patterns of cortical activity differing on the macro-column scale. Moreover, a recent study investigated the ability to differentiate cortical laminae with the use of different MEG models and a head-cast for minimizing head-movements (Troebinger et al., 2014). Therefore, a combination of an appropriate model at the appropriate cortical geometry can yield surprisingly good results.

Importantly, any estimate of MEG resolution will be influenced by the forward and inverse modeling required to transform the signals from the sensor level to the source level. Continuous head position recordings or even the usage of a head-casket or bite-bars is expected to improve the co-registration with the head-points and therefore the quality of the data recorded. Our results regarding the effect of dipole

orientation on resolution highlight the importance of using each subject's fMRI data to place the dipoles. If the anatomy used is based on an atlas, it is expected that the sources' placements will not be ideal and therefore the localization will be affected.

Although we used standard Brainstorm parameters in our modeling, other choices would likely have led to different conclusions about the level of crosstalk and point spread (Liu et al., 2002) shared by nearby sources. Similarly, our conclusions about resolution were determined by the assumption that the dipoles orientations were normal to the cortical surface and followed cortical curvature along the gyri and sulci. Moreover, the analysis that was performed in this study, reflects the resolution that can be achieved with a specific selection of methods; namely, the threshold applied to the signal amplitude and the stimulus that was projected.

Conclusion

MEG has traditionally been used in applications requiring excellent temporal resolution. However, its spatial resolution is most often considered to be coarse. We have shown that MEG can recover retinotopic maps with similar shape to those obtained with fMRI, and in some areas with comparable spatial resolution.

Acknowledgements

We would like to thank Elizabeth Bock for MEG training and help in data acquisition, François Tadel for valuable suggestions in using Brainstorm and Drs. Matthew Krause and Theodore Zanos for their comments on the data analysis and Dr. Reza Farivar-Mohseni for his help with fMRI surface rendering. This work was funded by a Molson Neuro-Engineering and a Gerry Sklavounos - MNA Laurier-Dorion Scholarship to K.N., and by a grant from NSERC (341534-12) to C.C.P. S.B. was supported by the Killam Foundation, a Senior-Researcher grant from the Fonds de Recherche du Québec - Santé (27605), a Discovery Grant from the National Science and Engineering Research Council of Canada (436355-13) and the NIH (2R01EB009048-05).

Appendix A. Supplementary material

Supplementary data associated with this article can be found in the online version at <http://dx.doi.org/10.1016/j.neuroimage.2016.10.017>.

References

- Aine, C.J., Stephen, J.M., 2003. Chapter 5 - MEG studies of visual processing. In: Posner, A.Z.M.P.I. (Ed.), *The Cognitive Electrophysiology of Mind and Brain*. Academic Press, San Diego, 93–142.
- Baillet, S., Mosher, J.C., Leahy, R.M., 2001. Electromagnetic brain mapping. *IEEE Signal Process. Mag.* 18, 14–30.
- Barth, D.S., Sutherling, W., Broffman, J., Beatty, J., 1986. Magnetic localization of a dipolar current source implanted in a sphere and a human cranium. *Electroencephalogr. Clin. Neurophysiol.* 63, 260–273.
- Benbadis, S.R., Beran, R.G., Berg, A.T., Jr, J.E., Galanopoulou, A.S., Kaplan, P.W., Koutroumanidis, M., Moshe, S.L., Jr, D.R.N., Serratos, J.M., et al., 2010. *Atlas of Epilepsies* (Springer Science & Business Media).
- de Boer, R., Kuyper, P., 1968. Triggered correlation. *IEEE Trans. Biomed. Eng.* 15, 169–179.
- Brainard, D.H., 1997. The psychophysics toolbox. *Spat. Vis.* 10, 433–436.
- Brookes, M.J., Zumer, J.M., Stevenson, C.M., Hale, J.R., Barnes, G.R., Vrba, J., Morris, P.G., 2010. Investigating spatial specificity and data averaging in MEG. *NeuroImage* 49, 525–538.
- Burkhalter, A., Essen, D.V., 1986. Processing of color, form and disparity information in visual areas VP and V2 of ventral extrastriate cortex in the macaque monkey. *J. Neurosci.* 6, 2327–2351.
- Cansino, S., Williamson, S.J., Karron, D., 1994. Tonotopic organization of human auditory association cortex. *Brain Res.* 663, 38–50.
- Cichy, R.M., Ramirez, F.M., Pantazis, D., 2015. Can visual information encoded in cortical columns be decoded from magnetoencephalography data in humans? *NeuroImage* 121, 193–204.
- Cicmil, N., Bridge, H., Parker, A.J., Woolrich, M.W., Krug, K., 2014. Localization of MEG human brain responses to retinotopic visual stimuli with contrasting source reconstruction approaches. *Brain Imaging Methods* 8, 127.
- Clavagnier, S., Dumoulin, S.O., Hess, R.F., 2015. Is the cortical deficit in amblyopia due to reduced cortical magnification, loss of neural resolution, or neural disorganization? *J. Neurosci.* 35, 14740–14755.
- Cottereau, B., Lorenceau, J., Gramfort, A., Clerc, M., Thirion, B., Baillet, S., 2011. Phase delays within visual cortex shape the response to steady-state visual stimulation. *NeuroImage* 54, 1919–1929.
- Dale, A.M., Sereno, M.I., 1993. Improved localization of cortical activity by combining EEG and MEG with MRI cortical surface reconstruction: a linear approach. *J. Cogn. Neurosci.* 5, 162–176.
- Dale, A.M., Fischl, B., Sereno, M.I., 1999. Cortical Surface-Based Analysis: I. Segm. Surface Reconstruct. *NeuroImage* 9, 179–194.
- Daniel, P.M., Whitteridge, D., 1961. The representation of the visual field on the cerebral cortex in monkeys. *J. Physiol.* 159, 203–221.
- Darvas, F., Pantazis, D., Kucukaltun-Yildirim, E., Leahy, R.M., 2004. Mapping human brain function with MEG and EEG: methods and validation. *NeuroImage* 23 (Supplement 1), S289–S299.
- Das, A., Gilbert, C.D., 1995. Long-range horizontal connections and their role in cortical reorganization revealed by optical recording of cat primary visual cortex. *Nature* 375, 780–784.
- DeAngelis, G.C., Ohzawa, I., Freeman, R.D., 1995. Receptive-field dynamics in the central visual pathways. *Trends Neurosci.* 18, 451–458.
- Dijkstra, E.W., 1959. A note on two problems in connexion with graphs. *Numer. Math.* 1, 269–271.
- DoCarmo, M., 1976. *Differential Geometry of Curves And Surfaces*, Pearson, Englewood Cliffs, N.J.
- Dougherty, R.F., Koch, V.M., Brewer, A.A., Fischer, B., Modersitzki, J., Wandell, B.A., 2003. Visual field representations and locations of visual areas V1/2/3 in human visual cortex. *J. Vis.* 3, 586–598.
- Dumoulin, S.O., Wandell, B.A., 2008. Population receptive field estimates in human visual cortex. *NeuroImage* 39, 647–660.
- Duncan, R.O., Boynton, G.M., 2003. Cortical magnification within human primary visual cortex correlates with acuity thresholds. *Neuron* 38, 659–671.
- Endo, S., Toyama, H., Kimura, Y., Ishii, K., Senda, M., Kiyosawa, M., Uchiyama, A., 1997. Mapping visual field with positron emission tomography by mathematical modeling of the retinotopic organization in the calcarine cortex. *IEEE Trans. Med. Imaging* 16, 252–260.
- Engel, S.A., Glover, G.H., Wandell, B.A., 1997. Retinotopic organization in human visual cortex and the spatial precision of functional MRI. *Cereb. Cortex* 7, 181–192.
- Felleman, D.J., Essen, D.C.V., 1987. Receptive field properties of neurons in area V3 of macaque monkey extrastriate cortex. *J. Neurophysiol.* 57, 889–920.
- Fischl, B., Sereno, M.I., Dale, A.M., 1999. Cortical surface-based analysis: II: inflation, flattening, and a surface-based coordinate system. *NeuroImage* 9, 195–207.
- Fischl, B., Liu, A., Dale, A.M., 2001. Automated manifold surgery: constructing geometrically accurate and topologically correct models of the human cerebral cortex. *IEEE Trans. Med. Imaging* 20, 70–80.
- Fox, P.T., Miezin, F.M., Allman, J.M., Essen, D.V., Raichle, M.E., 1987. Retinotopic organization of human visual cortex mapped with positron-emission tomography. *J. Neurosci.* 7, 913–922.
- Freeman, J., Simoncelli, E.P., 2011. Metamers of the ventral stream. *Nat. Neurosci.* 14, 1195–1201.
- Fyfan, F., Holliday, I.E., Singh, K.D., Anderson, S.J., Harding, G.F.A., 1997. Magnetoencephalographic investigation of human cortical area V1 using color stimuli. *NeuroImage* 6, 47–57.
- Gao, J.-H., Liu, H.-L., 2012. Inflow effects on functional MRI. *NeuroImage* 62, 1035–1039.
- Gattass, R., Sousa, A.P.B., Rosa, M.G.P., 1987. Visual topography of V1 in the Cebus monkey. *J. Comp. Neurol.* 259, 529–548.
- Goldenholz, D.M., Ahlfors, S.P., Hämäläinen, M.S., Sharon, D., Ishitobi, M., Vaina, L.M., Stufflebeam, S.M., 2009. Mapping the signal-to-noise-ratios of cortical sources in magnetoencephalography and electroencephalography. *Hum. Brain Mapp.* 30, 1077–1086.
- Hagler, D.J., Halgren, E., Martinez, A., Huang, M., Hillyard, S.A., Dale, A.M., 2009. Source estimates for MEG/EEG visual evoked responses constrained by multiple, retinotopically-mapped stimulus locations. *Hum. Brain Mapp.* 30, 1290–1309.
- Hämäläinen, M.S., Ilmoniemi, R.J., 1994. Interpreting magnetic fields of the brain: minimum norm estimates. *Med. Biol. Eng. Comput.* 32, 35–42.
- Hämäläinen, M., Hari, R., Ilmoniemi, R.J., Knuutila, J., Lounasmaa, O.V., 1993. Magnetoencephalography/char22{theory, instrumentation, and applications to noninvasive studies of the working human brain. *Rev. Mod. Phys.* 65, 413–497.
- Helmholtz, H., 1853. Ueber einige Gesetze der Vertheilung elektrischer Ströme in körperlichen Leitern mit Anwendung auf die thierisch-elektrischen Versuche. *Ann. Phys.* 165, 211–233.
- Holmes, G., 1945. Ferrier lecture: the organization of the visual cortex in man. *Proc. R. Soc. Lond. B Biol. Sci.* 132, 348–361.
- Horton, J.C., Hoyt, W.F., 1991. The representation of the visual field in human striate cortex: a revision of the classic holmes map. *Arch. Ophthalmol.* 109, 816–824.
- Huang, M.X., Mosher, J.C., Leahy, R.M., 1999. A sensor-weighted overlapping-sphere head model and exhaustive head model comparison for MEG. *Phys. Med. Biol.* 44, 423.
- Hubel, D.H., Wiesel, T.N., 1977. Ferrier lecture: functional architecture of macaque monkey visual cortex. *Proc. R. Soc. Lond. B Biol. Sci.* 198, 1–59.
- Hwang, J.-N., Lay, S.-R., Lippman, A., 1994. Nonparametric multivariate density estimation: a comparative study. *IEEE Trans. Signal Process.* 42, 2795–2810.
- Jeffreys, D.A., Axford, J.G., 1972. Source locations of pattern-specific components of human visual evoked potentials. II. Component of extrastriate cortical origin. *Exp.*

- Brain Res. 16, 22–40.
- Kaoru Seki, N.N., 1996. Neuromagnetic evidence that the P100 component of the pattern reversal visual evoked response originates in the bottom of the calcarine fissure. *Electroencephalogr. Clin. Neurophysiol.* 100, 436–442.
- Langner, G., Sams, M., Heil, P., Schulze, H., 1997. Frequency and periodicity are represented in orthogonal maps in the human auditory cortex: evidence from magnetoencephalography. *J. Comp. Physiol. A* 181, 665–676.
- Leahy, R.M., Mosher, J.C., Spencer, M.E., Huang, M.X., Lewine, J.D., 1998. A study of dipole localization accuracy for MEG and EEG using a human skull phantom.
- Lin, F.-H., Witzel, T., Ahlfors, S.P., Stufflebeam, S.M., Belliveau, J.W., Hämäläinen, M.S., 2006. Assessing and improving the spatial accuracy in MEG source localization by depth-weighted minimum-norm estimates. *NeuroImage* 31, 160–171.
- Liu, A.K., Dale, A.M., Belliveau, J.W., 2002. Monte Carlo simulation studies of EEG and MEG localization accuracy. *Hum. Brain Mapp.* 16, 47–62.
- Livingstone, M.S., Pack, C.C., Born, R.T., 2001. Two-dimensional substructure of MT receptive fields. *Neuron* 30, 781–793.
- Marmarelis, P.Z., Marmarelis, V.Z., 1978. The white-noise method in system identification. In: *Analysis of Physiological Systems*. Springer, US, pp. 131–180.
- Mineault, P.J., Zanos, T.P., Pack, C.C., 2013. Local field potentials reflect multiple spatial scales in V4. *Front. Comput. Neurosci.* 7, 21.
- Moradi, F., Liu, L.C., Cheng, K., Waggoner, R.A., Tanaka, K., Ioannides, A.A., 2003. Consistent and precise localization of brain activity in human primary visual cortex by MEG and fMRI. *NeuroImage* 18, 595–609.
- Nakamura, M., Kakigi, R., Okusa, T., Hoshiyama, M., Watanabe, K., 2000. Effects of check size on pattern reversal visual evoked magnetic field and potential. *Brain Res.* 872, 77–86.
- Okada, Y.C., Lahteenmäki, A., Xu, C., 1999. Experimental analysis of distortion of magnetoencephalography signals by the skull. *Clin. Neurophysiol.* 110, 230–238.
- Pack, C.C., Conway, B.R., Born, R.T., Livingstone, M.S., 2006. Spatiotemporal structure of nonlinear subunits in macaque visual cortex. *J. Neurosci.* 26, 893–907.
- Pantev, C., Hoke, M., Lehnertz, K., Lütkenhöner, B., Anogianakis, G., Wittkowski, W., 1988. Tonotopic organization of the human auditory cortex revealed by transient auditory evoked magnetic fields. *Electroencephalogr. Clin. Neurophysiol.* 69, 160–170.
- Pantev, C., Eulitz, C., Elbert, T., Hoke, M., 1994. The auditory evoked sustained field: origin and frequency dependence. *Electroencephalogr. Clin. Neurophysiol.* 90, 82–90.
- Pantev, C., Bertrand, O., Eulitz, C., Verkindt, C., Hampson, S., Schuierer, G., Elbert, T., 1995. Specific tonotopic organizations of different areas of the human auditory cortex revealed by simultaneous magnetic and electric recordings. *Electroencephalogr. Clin. Neurophysiol.* 94, 26–40.
- Pascual-Marqui, R.D., Michel, C.M., Lehmann, D., 1994. Low resolution electromagnetic tomography: a new method for localizing electrical activity in the brain. *Int. J. Psychophysiol.* 18, 49–65.
- Pelli, D.G., 1997. The VideoToolbox software for visual psychophysics: transforming numbers into movies. *Spat. Vis.* 10, 437–442.
- Perry, G., Adjajian, P., Thai, N.J., Holliday, I.E., Hillebrand, A., Barnes, G.R., 2011. Retinotopic mapping of the primary visual cortex – a challenge for MEG imaging of the human cortex. *Eur. J. Neurosci.* 34, 652–661.
- Pienaar, R., FISCHL, B., CAVINESS, V., MAKKRIS, N., GRANT, P.E., 2008. A methodology for analyzing curvature in the developing brain from preterm to adult. *Int. J. Imaging Syst. Technol.* 18, 42–68.
- Poghosyan, V., Ioannides, A.A., 2007. Precise mapping of early visual responses in space and time. *NeuroImage* 35, 759–770.
- Portin, K., Hari, R., 1999. Human parieto-occipital visual cortex: lack of retinotopy and foveal magnification. *Proc. R. Soc. B Biol. Sci.* 266, 981–985.
- Qiu, A., Rosenau, B.J., Greenberg, A.S., Hurdal, M.K., Barta, P., Yantis, S., Miller, M.I., 2006. Estimating linear cortical magnification in human primary visual cortex via dynamic programming. *NeuroImage* 31, 125–138.
- R Gattass, C.G.G., 1981. Visual topography of V2 in the Macaque. *J. Comp. Neurol.* 201, 519–539.
- Ringach, D., Shapley, R., 2004. Reverse correlation in neurophysiology. *Cogn. Sci.* 28, 147–166.
- Sarvas, J., 1987. Basic mathematical and electromagnetic concepts of the biomagnetic inverse problem. *Phys. Med. Biol.* 32, 11.
- Sereno, M.I., Dale, A.M., Reppas, J.B., Kwong, K.K., Belliveau, J.W., Brady, T.J., Rosen, B.R., Tootell, R.B., 1995. Borders of multiple visual areas in humans revealed by functional magnetic resonance imaging. *Science* 268, 889–893.
- Sethian, J.A., 1996. A fast marching level set method for monotonically advancing fronts. *Proc. Natl. Acad. Sci. U. S. A* 93, 1591–1595.
- Sharon, D., Hämäläinen, M.S., Tootell, R.B.H., Halgren, E., Belliveau, J.W., 2007. The advantage of combining MEG and EEG: comparison to fMRI in focally stimulated visual cortex. *NeuroImage* 36, 1225–1235.
- Smith, A.T., Singh, K.D., Williams, A.L., Greenlee, M.W., 2001. Estimating Receptive Field Size from fMRI Data in Human Striate and Extrastriate Visual Cortex. *Cereb. Cortex* 11, 1182–1190.
- Stephen, J.M., Aine, C.J., Christner, R.F., Ranken, D., Huang, M., Best, E., 2002. Central versus peripheral visual field stimulation results in timing differences in dorsal stream sources as measured with MEG. *Vision. Res.* 42, 3059–3074.
- Sutherling, W.W., Akhtari, M., Mamelak, A.N., Mosher, J., Arthur, D., Sands, S., Weiss, P., Lopez, N., DiMauro, M., Flynn, E., et al., 2001. Dipole localization of human induced focal afterdischarge seizure in simultaneous magnetoencephalography and electrocorticography. *Brain Topogr.* 14, 101–116.
- Tadel, F., Baillet, S., Mosher, J.C., Pantazis, D., Leahy, R.M., 2011. Brainstorm: a user-friendly application for MEG/EEG analysis, brainstorm: a user-friendly application for MEG/EEG analysis. *Comput. Intell. Neurosci.* 2011 (2011), e879716.
- Tesche, C.D., Uusitalo, M.A., Ilmoniemi, R.J., Huotilainen, M., Kajola, M., Salonen, O., 1995. Signal-space projections of MEG data characterize both distributed and well-localized neuronal sources. *Electroencephalogr. Clin. Neurophysiol.* 95, 189–200.
- Troebinger, L., López, J.D., Lutti, A., Bestmann, S., Barnes, G., 2014. Discrimination of cortical laminae using MEG. *NeuroImage* 102 (Part 2), 885–893.
- Uusitalo, M.A., Ilmoniemi, R.J., 1997. Signal-space projection method for separating MEG or EEG into components. *Med. Biol. Eng. Comput.* 35, 135–140.
- Van Essen, D.C., Newsome, W.T., Maunsell, J.H.R., 1984. The visual field representation in striate cortex of the macaque monkey: asymmetries, anisotropies, and individual variability. *Vision. Res.* 24, 429–448.
- Wandell, B.A., Dumoulin, S.O., Brewer, A.A., 2007. Visual field maps in human cortex. *Neuron* 56, 366–383.
- White, B.R., Culver, J.P., 2010. Phase-encoded retinotopy as an evaluation of diffuse optical neuroimaging. *NeuroImage* 49, 568–577.
- Zeki, S.M., 1978. Uniformity and diversity of structure and function in rhesus monkey prestriate visual cortex. *J. Physiol.* 277, 273–290.